THE JOURNAL OF PHYSICAL CHEMISTRY B

Article

pubs.acs.org/JPCB

Limit of Miscibility and Nanophase Separation in Associated Mixtures

P. A. Artola,*[,†] A. Raihane,[‡] C. Crauste-Thibierge,[‡] D. Merlet,[¶] M. Emo,[§] C. Alba-Simionesco,*[,∥] and B. Rousseau*[,⊥]

[†]Laboratoire de Chimie-Physique, Université de Paris-Sud, Orsay, France

[‡]Laboratoire Léon Brillouin, CNRS, CEA, Saclay, France

[¶]Institut de Chimie Moléculaire et des Matériaux d'Orsay, Université de Paris-Sud, Orsay, France

[§]Institut J. Barriol, CNRS, Université de Lorraine, Vandoeuvre-lès-Nancy cedex, France

[∥]Laboratoire Léon Brillouin, CEA, CNRS, Saclay, France

[⊥]Laboratoire de Chimie-Physique, Université de Paris-Sud, CNRS, Orsay, France

Supporting Information

ABSTRACT: We present a detailed analysis of the mixing process in an associating system, the water−*tert*-butanol (2-methyl-2-propanol) mixture. Using molecular dynamics simulations, together with neutron, X-ray diffraction experiments, and pulsed gradient spin−echo NMR, we study the local structure and dynamic properties over the full concentration range, and thereby provide quantitative data that reveal relationships between local structure and macroscopic behavior. For an alcohol-rich mixture, diffraction patterns from both neutron and X-ray experiments exhibit a peak at low wavelength vector ($q \approx 0.7$ Å^{-1}) characteristic of supermolecular structures. On increasing the water content, this "prepeak" progressively flattens and shifts to low wave vector . We identify hydrogen bonds in the system as the driving force for the specific organization that appears in mixtures, and provide an analysis of the variation of the cluster size distribution with composition. We find that the sizes of local hydrogen-bonded clusters observed in alcohol-rich mixtures become larger as the mole fraction, x_w, of water is increased; a nanophase separation is seen for x_w in the range 0.6−0.7. This corresponds to several changes in some macroscopic properties of the liquid mixture. Thus, we propose a microscopic description of the effect of water addition in alcohol, which is in agreement with both neutron diffraction pattern and mobility of water and alcohol species. In summary we present a full and comprehensive description of miscibility at its limit in an associated system.

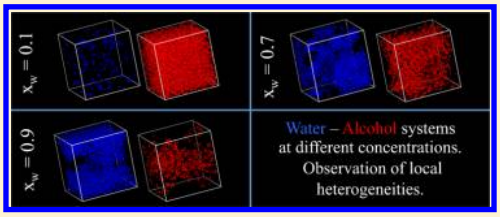

INTRODUCTION

Understanding mixing processes and mixing properties in associated fluids has known a growing interest these past years.[1−8] Several important issues have guided these studies, among which for instance water purification, pharmaceutical formulation of medicines, biological modeling of cell systems, and general behavior of biological molecules.[9] All these various phenomena are, in the first place, guided by one of the most specific properties of water: the orientational and strong hydrogen bonding interaction. A large amount of work has been dedicated to describe its chemical basis and its properties, in particular in more recent studies in mixtures[10] and biological systems.[11,12] It has been a well-known feature that, although all liquids are heterogeneous at short-range,[13] associated systems, and above all water, present at very short-range an excess of density probability of finding a molecule around another one due to the hydrogen bond. This specific behavior can be seen in a first maximum in the radial distribution function very close to zero (shorter than a van der Waals radius for instance) followed by a more "usual" dispersion maximum.[14] By integration of this first maximum in pure water liquid at ambient conditions one may find that the number of water molecules at hydrogen bonding distance is around 4.5 and a usual coordination number (around 10) after integration of the two first maxima. Such specific phenomena are now known in several other systems such as alcohols or amines but with a moderated intensity. Monoalcohols present furthermore the specificity to possess both hydrophobic alkane chains and a polar hydrophilic site that can be involved in hydrogen bonding interactions. This balance between hydrophilic and hydrophobic behavior in a single molecule is widely used in self-assembly systems as surfactant for instance. In this work we study water alcohol mixing properties for short-chain alcohols to avoid self-assembly behavior and to ensure miscibility, but not too short to emphasis the hydrophobic to hydrophilic balance. The water−*tert*-butanol mixture presents all these required properties.

An important feature that led our work and which accounts for a large part of our results is the specific structural heterogeneities that arise in associated mixtures. These

Received: December 18, 2012
Revised: July 11, 2013
Published: August 12, 2013

dx.doi.org/10.1021/jp3124499 | *J. Phys. Chem. B* 2013, 117, 9718−9727

heterogeneities have long been suspected[15−17] to be responsible for macroscopic unusual behaviors but, as far as we know, their link with macroscopic quantities has not been clearly quantified in associated mixtures. Although a structural analysis is important (for example using radial distribution functions), one must try to understand in which way local heterogeneities affect macroscopic properties. Such heterogeneities may be seen, as we show, as nanophase separation in the system. Also all the analysis of mixing properties in associated fluids has to link macroscopic properties to the local specific structure, which is the fingerprint of hydrogen bonding effects and of the hydrophilic−hydrophobic balance. A typical example of these macroscopic properties is the very well-known maximum of the viscosity of associated mixtures[18−20] such as ethanol−water or propanone−water with concentration.

In this spirit, this work presents experimental and molecular simulation results of both microscopic and macroscopic properties. Water−*tert*-butanol mixtures were investigated by neutron and X-ray scattering, pulsed gradient spin−echo NMR, and molecular simulation to obtain its local structure and various macroscopic properties. This work is therefore based on the role of interactions, more specifically cross-interactions, between unlike molecules and the balance between hydrophobic and hydrophilic effects, to make a link between local structure and macroscopic properties.

In this paper we report our simulation and experimental methods before presenting the local structure of the mixture and the microscopic interpretation. We conclude with the link between the microscopic scale and the macroscopic behavior.

SIMULATION DETAILS

We used classical molecular dynamics simulations; we present the various details of these simulations in this section.

Interaction Potentials. Several authors have developed force fields dedicated to the study of water−*tert*-butanol mixtures. Ferrari et al.[15] have proposed a force field for alcohols based on the Williams crystal force field parameters and to be used with the TIP3P water model. However, density under ambient conditions for ethanol is underestimated by 8%, and density of pure *tert*-butanol is underestimated by 3%. A few mixture densities have been computed with discrepancies of the order of 3%.

Lee and van der Vegt[5] have proposed a force field parametrized to reproduce experimental Kirkwood−Buff integrals over a large composition range, at room temperature and atmospheric pressure. The force field has been optimized by using a reaction field approach to handle electrostatic interactions.

We chose the water TIP4P/2005 model[21] because it is in agreement with many water properties, including thermodynamics, structural, and dynamical properties, and yet is a simple classical potential (no polarization, no explicit H-bond term, etc.). The TraPPE-United Atoms (TraPPE-UA) model,[22,23] optimized to reproduce liquid−vapor phase equilibria, is in general very satisfactory with mean errors of about 1% for the saturated liquid densities and normal boiling points and errors of 1.5% and 3% for critical temperatures and densities, respectively.[22] We have checked that volumetric properties of the water TIP4P/2005 and *tert*-butanol TraPPE-UA models are well predicted over the full concentration range: excess volume deviation from experimental data is smaller than 0.4 cm^3/mol, and the deviation for the total molar volume is smaller than 0.2% (see the Supporting Information for more details), although simple Lorentz−Berthelot combination rules have been used for the Lennard-Jones potential cross parameters:

$$\varepsilon_{ij} = \sqrt{\varepsilon_{ii}\varepsilon_{jj}}$$

$$\sigma_{ij} = \frac{\sigma_{ii} + \sigma_{jj}}{2}$$

We used a Lennard-Jones cutoff of 15 Å, and an electrostatic cutoff taken as half the box size. Long range interactions for the Lennard-Jones potential were calculated using an homogeneous approximation and long-range electrostatic interactions were calculated using Ewald summation method.[24]

MD SIMULATION DETAILS

Sampling in associated systems can be challenging, great care must be taken. Molecular dynamics simulations were performed by using our locally build Newton package.[25] We simulated 11 different compositions (from pure alcohol to pure water with a molar fraction increment of 0.1). Each system contained 2000 molecules. Water was described as a rigid body. Covalent bonds in *tert*-butanol were constrained by using the RATTLE algorithm with a relative tolerance set to 10^{-10}. The time step was chosen as 1 fs.

We performed *NpT* Berendsen simulations (1 ns of equilibration, 10 ns of production) in order to compute thermodynamical properties and *NVT* Nosé−Hoover simulations (1 ns of equilibration and 30 ns of production), using the density obtained from the *NpT* simulations, for structure and transport properties. The temperature and pressure chosen were respectively T = 308.15 K and $p = 10^5$ Pa. The barostat and thermostat time constants were set equal to 0.1 ps for *NpT* simulations. *NVT* simulations used a Nosé−Hoover chain of 10 segments and a time constant value equal to 0.1 ps.

Simulations were done in a cubic box with use of so-called periodic boundary conditions and minimum image convention. To compute structural properties ($g(r)$, $S(q)$ and cluster analysis) and mean-squared displacement, trajectory files including particle positions were written every 50 fs. The stress tensor (required for the viscosity) was written every 5 fs.

EXPERIMENTAL SETUP DETAILS

Neutron scattering experiments were performed on the D7 spectrometer at the Institute Laüe-Langevin in Grenoble (France). The main advantage of this instrument is its ability to separate the coherent scattering (containing the structural information) from incoherent scattering by using a technique of longitudinal neutron polarization analysis.[26] The incoherent scattering can be used as an internal calibration since it is proportional to the quantity of matter present under the beam and contains all the geometric effects (auto-absorption, scattering volume effects, ...). In this way we easily obtain the coherent scattering signal in absolute units ($barn \cdot str^{-1} \cdot molecule^{-1}$). To be precise, this calibration on other spectometers needs perfect knowledge of the volume of the sample under the neutron beam and to put exactly the same volume and the same geometry of vanadium under the beam. Since the coherent and incoherent signal are measured simultaneously on the same sample, normalization to the incoherent signal resolves this problem, we only need to know the tabulated incoherent cross section of the sample along with its deuteration level. Vanadium is then simply used to correct the detectors' efficiency since its spectrum is perfectly flat on

dx.doi.org/10.1021/jp3124499 | J. Phys. Chem. B 2013, 117, 9718−9727

the D7 q range. At very low scattering vector the measurements agree very well with the theoretical limit of coherent scattering for all the mixtures:

$$\lim_{q\to 0} S_{coh}(q) = (\sum_i b_i)^2 k_B T \rho \chi_T$$

with χ_T, ρ, and b_i respectively the isothermal compressibility, the number density of the liquid at the temperature T, and the coherent scattering length of the nucleus i summed over the entire molecule or the unit averaged on the specific concentration of a mixture.

At high q values, the total coherent scattering cross sections of the current mixtures are fully compatible with the experiments performed over the limited q range with

$$\lim_{q\to\infty} S_{coh}(q) = \frac{\sigma_{coh}}{4\pi}$$

These latter values were used to normalized all the spectra to 1 at high q in Figure 2 and compared to the calculated ones. Several mixtures of deuterated *tert*-butanol ($(CD_3)_3COD$, at 98.4% D) and heavy water (D_2O, at 100% D) were prepared (Table 1). Measurements were performed at T = 300 K by

Table 1. Numerical Values of Neutron Scattering Constants for the Different Mixtures of *tert*-Butanol and Water (x mole fraction)[a]

x[b]	σ_{incoh}[b]	σ_{coh}[b]	$S_{coh}(q\to\infty)$[c]	$S_{coh}(q\to 0)$[c]
0	33.0	81.7	6.5	2.7
0.116	29.7	74.0	5.9	2.3
0.3	24.3	61.2	4.9	1.8
0.5	18.6	48.6	3.9	1.2
0.709	12.5	34.7	2.8	0.74
0.89	7.2	22.6	1.8	0.4
1	4.1	15.4	1.2	0.24

[a]The deuteration rate of *tert*-butanol was taken equal to 98.4% and water at 100%. The scattering cross-section σ and the intensity of the coherent scattering S_{coh} is given in absolute units at T = 300 K. [b]Mole fraction of water. [b]Units: barn. [c]Units: barn·structure^{-1}·molecule^{-1}.

using an alumina annular cell of 0.5 mm thickness and a mean diameter of 19.5 mm. A wavelength of 4.8 Å was chosen to focus on the small q-range 0.1 Å^{-1} < q < 2.4 Å^{-1}.

Hydrogenated samples $(CH_3)_3COH$ + H_2O with the same molar fraction as above were studied by small-angle X-ray scattering (SAXS); the experiments were performed at 293 and 303 K to avoid crystallization of *tert*-butanol. Data were collected on a "SAXSess mc^2" instrument (Anton Paar), using a line-collimation system. This instrument is attached to a ID 3003 laboratory X-ray generator (General Electric) equipped with a sealed X-ray tube (PANalytical, $\lambda_{CuK\alpha}$ = 0.1542 nm) operating at 40 kV and 50 mA. Each sample was introduced in a "Special Glass" capillary (Φ = 1.5 mm, W. Müller*Glas*), inside an evacuated sample chamber, and exposed to the X-ray beam for 5 min. With use of *SAXSQuant* software (Anton Paar), the 2D image was integrated into one-dimensional scattering intensities $I(q)$ as a function of the magnitude of the scattering vector q. Thanks to a translucent beam-stop allowing the measurement of an attenuated primary beam at q = 0, all measured intensities can therefore be calibrated by normalizing the attenuated primary intensity. All data were then corrected for the background scattering from the empty capillary and for slit-smearing effects by a desmearing procedure from SAXSQuant software by using the Lake method. After correction, obtained intensities are scaled into absolute units by using water as a reference material. From this point the coherent structure factor will be referred to as the "structure factor" and noted simply $S(q)$.

Viscosity measurements were also performed to cover the temperature range of the structural experiments; a standard "cylindrical Couette" apparatus is used: CONTRAVES Low-Shear30 with inner diameter of 11 mm and outer diameter of 12 mm. The data were compared to the data available in the literature at high temperature.[27] The viscosity is presented in the Supporting Information.

We measured self-diffusion constants using Pulsed Field Spin Echo NMR (PGSE-NMR). The PGSE-NMR experiments were performed on a Bruker Avance NMR 400 spectrometer with a broadband probe equipped with three-axis gradient coils without field/frequency lock control. The maximum gradient values for the z constant field direction was G_z = 45 G/cm, using a sine shape. Temperature was calibrated by using a reference ethylene glycol sample and controlled at 308 K with a Bruker BVT3000 system (1 K regulation).

Self-diffusion was measured with the double pulsed field gradient stimulated echo and LED sequence, using three spoil gradients.[28,29] Self-diffusion coefficients were determined from the classical Stejskal−Tanner equation:

$$\ln\left(\frac{I}{I_0}\right) = -DG^2\gamma^2\delta^2\left(\Delta - \frac{\delta}{3}\right)$$

where G is the magnitude of the four gradient pulses, Δ is the time interval between these pulses and δ is their duration, γ is the gyromagnetic ratio of the nucleus under study (here the proton), and I and I_0 are the integrated intensities of the signals obtained, with and without gradient pulses, respectively. The magnitude of the pulsed field gradient was varied between 2% and 95% of the maximum available value in 32 steps; the diffusion time Δ between two pulses was fixed at 100 ms, and the pulse duration δ was set to 2 ms. For the ^{1}H PGSE-NMR experiments, 8 scans were added at each step, with a relaxation delay of 2 s.

MISCIBILITY AND LOCAL STRUCTURE: A MICROSCOPIC INTERPRETATION

A first, but necessary, step consists of not only comparing experiments and simulations but also using what is specific to them (large time and space scales available in experiment and direct calculations of radial distribution functions in simulations for instance) to access to a wider view of the various phenomena specific to these associated systems. Neutron and X-ray scattering structure factors were calculated from trajectories using the following expression:[30]

$$S_T(q) = \frac{1}{\overline{b}^2}\left[\frac{1}{N}\left\langle\left|\sum_i b_i e^{i\mathbf{q}\cdot\mathbf{r}_i}\right|^2\right\rangle_t - (\overline{b^2} - \overline{b}^2)\right]$$

with $S_T(q)$ the total scattering structure factor, $\mathbf{q}$ the wave vector, $S(q)$ the structure factor, N the number of diffusing sites, b_i the scattering length of atom i, and $\mathbf{r}_i$ its position vector, and:

$$\overline{b}^2 = |\sum_\alpha c_\alpha b_\alpha|^2$$

dx.doi.org/10.1021/jp3124499 | J. Phys. Chem. B 2013, 117, 9718−9727

$$\overline{b^2} = \sum_{\alpha} c_\alpha b_\alpha^2$$

with α the diffusion center type and c_α its concentration. TraPPE-UA model uses united atoms in which a single point can represent a CH_3- group. Hydrogen positions (needed in the $S(q)$ calculation) are computed from the knowledge of carbon positions and simple trigonometric rules. Selected data are presented in the paper whereas the Supporting Information contains the remaining data. As all the structure information appears in the coherent term $S_{coh}(q)$ we will show the results for this term only:

$$S_{coh}(q) = \frac{1}{\overline{b}^2}\left[\frac{1}{N}\left\langle \left| \sum_i b_i e^{i\mathbf{q}\cdot\mathbf{r}_i} \right|^2 \right\rangle_t\right]$$

We present in Figure 1 the normalized coherent structure factor obtained from both neutron and X-ray scattering from

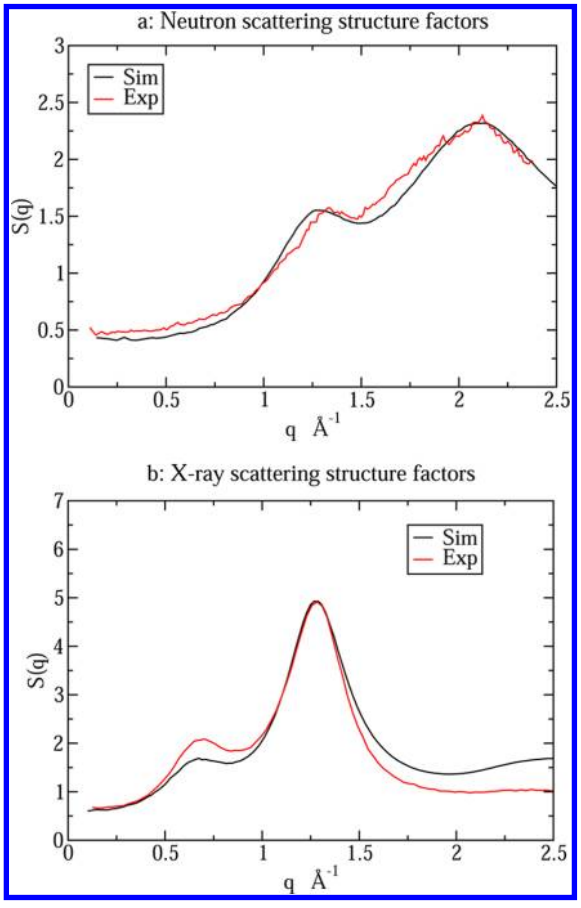

Figure 1. (a) Both experimental and simulation normalized scattering structure factors for water and *tert*-butanol at the water molar fraction of $x_w = 0.9$. (b) X-ray scattering structure factors (in arbitrary units) for a water and *tert*-butanol at the water mole fraction of $x_w = 0.3$.

experiments and from our simulations for two compositions. We notice a very good agreement between experiments and simulations. Furthermore, Figure 2 presents the structure factor for all compositions from both experiment and simulation. Three different main maxima can be identified on the curves:

(a) A first peak (usually called the "prepeak"[31,32]) around 0.7 Å^{-1} for the lowest concentration in water, which corresponds to a superstructure in the fluid mixture due to cluster correlations

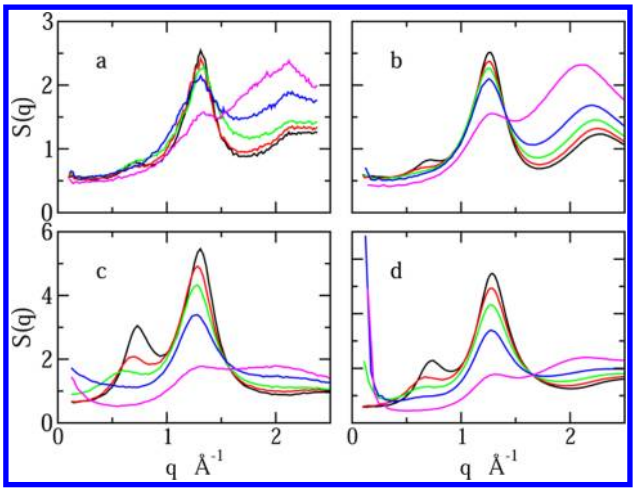

Figure 2. Structure factors: black, red, green, blue, and magenta represent respectively water molar fractions 0.1, 0.3, 0.5, 0.7, and 0.9: (a) experimental by neutrons, (b) simulated by neutrons, (c) experimental by X-rays and (d) simulated by X-rays.

already existing in the pure *tert*-butanol. This peak is bigger in the X-ray than in the neutron curves as the oxygen has a large electronic density around it and furthermore the local structure arises from oxygen atoms and their hydrogen bounds. As the proportion of water increases this maximum decreases and shifts to lower q, which means the various clusters are at greater distances or/and of greater sizes or, more probably, a mixture of both. Above the equimolar mixture the signature of correlated supermolecular structures disappears. We reproduce this effect by simulation but we see the disappearance of the prepeak already for the equimolar mixture in the neutron structure factor. This last observation indicates that potentials used in this simulation might not be attractive enough to maintain clusters as they should in the system for the equimolar mixture.

(b) A peak around 1.25 Å^{-1}, which corresponds to the first shell of alcohols in the mixture and obviously decreases as the molar fraction of water increases.

(c) A peak around 2.20 Å^{-1}, which corresponds to the first shell of water and some alcohol intramolecular correlations. This last peak increases with the molar fraction of water as expected.

Let us now focus on the prepeak, which accounts for supermolecular structures in the pure alcohol and at low water mole fraction. As the water proportion is increased, the prepeak appears at lower wavelength number, meaning larger sizes. This indicates that water molecules go in between these structures and/or form larger clusters with alcohol molecules, modifying their chemical nature. Both experimental and simulated X-ray structure factors increase quickly at high water proportions for very low q. This would indicate a very large structure. Liquid–liquid phase transition has not been reported for this system[33] but it could be a signature of a large nanophase separation. Indeed people agree in the literature on specific heterogeneities in associated mixtures but with various explanations for their origins and effects on macroscopic properties.[34,35]

We propose here a plausible chemical nature of the prepeak: we computed from simulations the number of clusters of size i (being the number of molecules included in these structures). An analysis in terms of cluster size distribution is done from trajectories. If two atoms in two different molecules are at a distance smaller than some cutoff value R_c, they are considered

dx.doi.org/10.1021/jp3124499 | J. Phys. Chem. B 2013, 117, 9718–9727

to belong to the same cluster. For a given instantaneous configuration, we compute the number of clusters of size i at time t, $N_c(i,t)$. This was done based on hydrogen bonded criteria between all types of molecules. We used oxygen positions of water and *tert*-butanol molecules rather than center of mass positions to compute cluster size distributions. The average number of clusters of size i, $N_c(i)$, is computed as a time average of $N_c(i,t)$ over 2.5 ns. Then we obtain the probability, $P_c(i)$, of a molecule to be in a cluster of size i by a normalization of N_c:

$$P_c(i) = \frac{N_c(i)}{N_c^T}$$

with N_c^T the total number of clusters in the fluid, obtained by integration:

$$N_c^T = \int_0^{i_{max}} \mathrm{d}i N_c(i)$$

with i_{max} obviously smaller than N_{tot}. We used a cutoff value R_c = 3.52 Å, which corresponds to the largest distance value of the first minimum in the oxygen−oxygen radial distribution function. This value changes with composition in the range 3.30−3.52 Å. A sensitivity analysis (presented in the Supporting Information) to R_c shows small differences in cluster size distribution without altering the conclusions of this study. Distance, energy, and bond angle criteria for H-bond are well-defined in pure water and have been used to study H-bond networks in water. This is less obvious in mixtures. The way to characterize clusters is then unfortunately system dependent. We expect typical structure induced by hydrogen bond at these sizes (corresponding to 0.7 $Å^{-1}$ and decreasing as the water mole fraction increases) to be responsible of the prepeak in the structure factor of the X-ray or neutrons. We present in Figure 3 the results for small cluster sizes. We observe that a structure

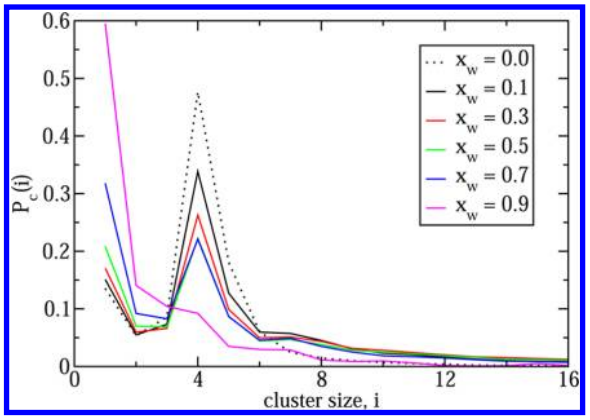

Figure 3. Probability of a molecule to belong to a cluster of size i as a function of cluster size. Simulated systems contain 2000 molecules. Pure alcohol distribution is shown as a reference.

including four different molecules (of either types) is the most favorable (and so forth stable) structure in the system as was reported for the pure alcohol: two papers,[36,37] related to this aspect, study mixtures of *tert*-butanol with different experimental techniques. A majority of cyclic structures, mostly formed by four molecules, is observed. As water mole fraction increases, the fraction of four molecule clusters decreases and larger and more dispersed structures appear (in other words the distribution of super molecular sizes is wider). At some point we only observe large (percolated) structures in the fluid. To show this directly, we represent in Figure 4 the fraction of molecules belonging to clusters of size smaller than i as a function of the size i of these clusters, $f_c(i)$, defined as:

$$f_c(i) = \frac{1}{N_{mol}} \sum_{m=1}^{i} m N_c(m)$$

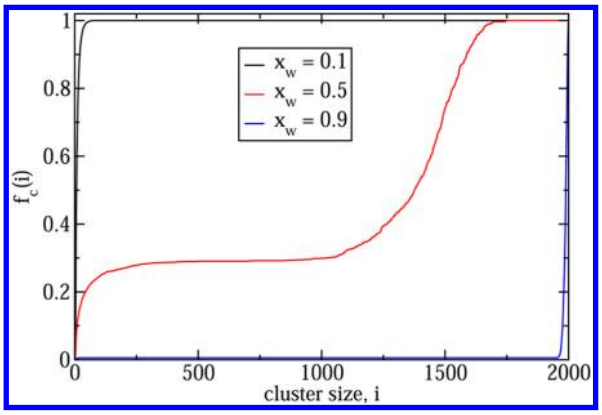

Figure 4. Fraction of molecules belonging to a cluster of size smaller or equal to i (normalized to the total number of molecules) as a function of the cluster size i.

For instance, a $f_c(i)$ value of 0.3 means that 30% of the molecules belong to a cluster of size smaller or equal to i. At low water mole fraction all the molecules belong to small clusters whereas for high water mole fraction all molecules percolate in a macroscopic structure typical of the pure water. For the equimolar mixture, $f_c(i)$ remains constant for i in the range 250−1000, which means there is no cluster of these sizes. This indicates the presence of a bimodal cluster size distribution with both small clusters and also larger structures.

From these results we propose these typical structures (from four alcohol molecules in the pure alcohol to larger structures in the mixtures) to be responsible for the prepeak and its evolution with concentration. Indeed as water mole fraction increases the average size of the objects increases too. Their correlations in the structure factor will appear at larger distances, in other words at smaller wavenumber. Furthermore, the width of the prepeak increases with water mole fraction and in the meantime its intensity decreases, in full agreement with what we see in the simulated cluster repartition: the addition of water in the mixture creates larger structures and also increases the width of the distribution. This is in good agreement with what was already observed[8,38−40] by neutron scattering at very low or very high concentration studies only.

From a modeling point of view, we can see that the potentials used give satisfactory results except around equimolar mixtures, at least for structural data. This can be easily understood as we used Lorentz−Berthelot mixing rules with potential parameters obtained for pure components. This so-called "transferability" of potential parameters shows here its limits, especially for associated mixtures in which local structure will dramatically affect polarizability and therefore electronic properties, in particular of the water. As a consequence we have a very good agreement between simulations and experiments except around the equimolar mixture.

What would be interesting now is to analyze the way the system goes from small clusters to a large percolated system. An

dx.doi.org/10.1021/jp3124499 | J. Phys. Chem. B 2013, 117, 9718−9727

interesting method for cluster analysis consists of an analysis of cluster distributions (one may see this as a radial distribution function of clusters[34]). We selected another route: we computed all radial distribution functions between all atoms and between center of masses. Although much information is included in these data they are difficult to comment on one by one and usually require having all of them on sight to be interpreted. Therefore an integrated form of these results is easier for physical interpretation. A first attempt could be to calculate Kirkwood−Buff integrals over all the accessible[13,41−43] pair distances. Indeed, as can be seen in the Supporting Information, radial distribution functions are far from being homogeneous at half the box size. This approach requires data for long-range correlations that cannot be accessible directly from simulations and require either very large boxes[44] or analytical treatments.[35] Another way consists of integrating the radial distribution functions up to the first shell in the liquid.[45,46] Hence, the integration of the hydrogen bond first peak will give us the hydrogen bonded coordination number.

The local structure, and in particular microscopic heterogeneities due to association, is mainly determined by how molecules interact with each other. These structures are involved at the mesoscopic range in the fluid and affect macroscopic behavior of the fluid in various ways. Let us state here that, although we do observe dramatic effects on transport properties (for instance the maximum of viscosity in water and alcohol mixtures, which can be three times the value of the viscosity of water in the water−ethanol mixture) excess thermodynamic properties in such systems can be quite small. Indeed typical excess enthalpies for water and alcohol mixtures show small excess properties (less than 1 kJ/mol to be compared to all other energetic terms in the system; for more details, see the Supporting Information).[35,47]

We computed the center of mass radial distribution functions for the three pairs: water−water, alcohol−alcohol and, the more interesting, alcohol−water that shows how the two species mix. From these curves the coordination number is therefore calculated following the formula:

$$N_i^j = \rho_i \int_0^{r_0} 4\pi r^2 g_{ij}^{\mathrm{cm}}(r)\, \mathrm{d}r$$

with ρ_i the number density of species i in the fluid, r_0 the radius of the coordination sphere, and $g_{ij}^{\mathrm{cm}}(r)$ the radial distribution function of the center of masses between species i and j. This number can also be seen as the number of "association" sites occupied for each species. The r_0 value chosen depends on the concentration but typical values (here for the equimolar system) are 5.00, 4.30, and 3.40 Å respectively for alcohol/alcohol, alcohol/water, and water/water coordination sphere radius. Radial distribution functions, $g_{ij}(r)$, were calculated from trajectories by calculating a histogram of probability density to find species (atom or molecule) j around a species i as:

$$g_{ij}(r) = \frac{1}{4\pi r^2 \rho_i} \frac{\mathrm{d}N_i^j(r)}{\mathrm{d}r}$$

with $\mathrm{d}N_i^j(r)$ the number of species j inside the sphere layer between r and $r + \mathrm{d}r$ around species i. Some of the radial distribution functions are presented in the Supporting Information . We present in Figures 5 and 6 the number of alcohol and water molecules hydrogen bonded to another molecule. We note that the total number of association sites is around 4.6 for water and 2 for the alcohol. This last feature is

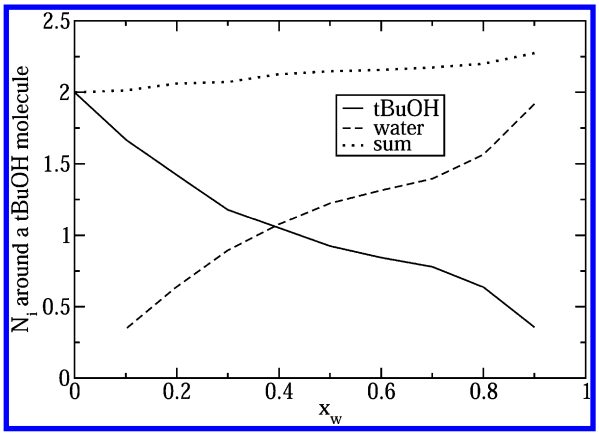

Figure 5. Number of water and *tert*-butanol around a given *tert*-butanol molecule and the sum of the two curves.

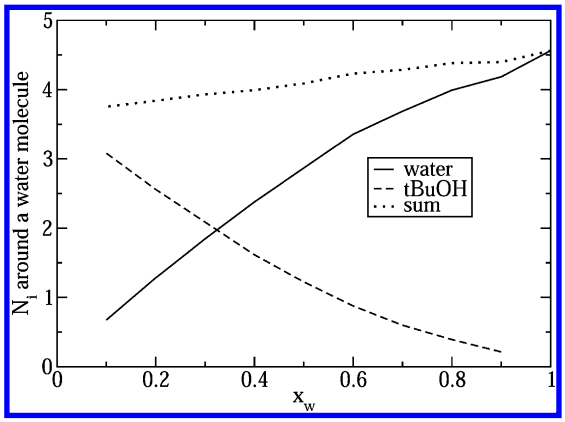

Figure 6. Number of water and *tert*-butanol around a given water molecule and the sum of the two curves.

interesting as it shows that for alcohol there is only one hydrogen bond site on the oxygen compared to two sites for the water oxygen. We furthermore note that this occupied association site number slowly increases with the water proportion in the system. This is mainly due to a density effect: the molar volume slowly decreases so molecules are globally closer to each other.

Both curves show logically that there is an increasing value of water around a given species when the proportion of water increases and respectively for the alcohol. But there is an interesting feature on the coordination number of the alcohol (cf. Figure 5): it shows a change in the concavity. We can give a microscopic interpretation of this phenomenon: if we consider a pure *tert*-butanol fluid and we add some water we note at low water mole fraction that there is an "excess" of water molecules hydrogen bonded to the alcohol. This clearly means that it is energetically more favorable to hydrogen bond a water molecule to the alcohol at infinite dilution of water. Once a water molecule is H-bonded to an alcohol molecule the question that arises is where the second water molecule added in the system will go. Figure 6 clearly shows that a water molecule will always prefer to be with other water molecules. Consequently, the second water molecule will hydrogen bond on the alcohol but in a way it can also be H-bonded to another water molecule. So forth, and typical snapshots of the system clearly show this, we observe for small water molar fractions various clusters of water molecules hydrogen bonded on the alcohol structure in the fluid (see the Supporting Information

dx.doi.org/10.1021/jp3124499 | J. Phys. Chem. B 2013, 117, 9718−9727

for more details). We mentioned earlier that there are only two association sites on the alcohol molecule so, at some point when adding water, all the association sites of the alcohol are already occupied by the water. Therefore all the "new" water molecules added in the system have the choice to keep to themselves or solvate within the hydrophobic part of the alcohol. As one could expect water would rather keep to itself and, above some specific water mole fraction, the alcohol will be forced to bind with itself. We can simply estimate this specific molar fraction: all sites of the alcohol are occupied if the number of water molecules is twice the number of alcohol molecules, and the behavior changes for a water mole fraction $x_w^c \approx 2/3$. Therefore the system goes from reverse micelles-like structures at low water mole fraction to usual micelles-like structures above this specific molar fraction. At low alcohol concentration ($x_w = 0.9$), we observed a behavior similar to the one described by Soper and collaborators,[48] i.e., the domination of nonpolar to nonpolar solute contacts. Concerning this aggregation behavior, Ferrari et al.,[15] at $x_w = 0.89$ and 0.39, observe dimers or small rings. Gupta and Patey[44] have done extensive simulations at low alcohol concentrations, using various force fields (e.g., Gromos-UA−SPC/E, Charmm−TIP3P, OPLS-AA−SPC/E, and LV-V-UA−SPC/E) and concluded that the Lee and van der Vegt force field, or the OPLS-AA force field, used with the SPC/E water model, do not exhibit aggregation at x_w above 0.94 whereas GromosUA/SPC/E or CharmmAA/TIP3P do.

As can be seen in Figure 5 the concavity change occurs for the water mole fraction somewhere between 0.6 and 0.7. This observation on the mixing behavior between the two species led to a very important fact: once all the association sites of the alcohol are occupied by water molecules two kinds of water molecules can be defined: the first one, bonded to the alcohol, can be seen as "adsorbed-like" water molecules and all the others are "bulk-like" water molecules. Therefore, above this specific water mole fraction, the fluid mixture is constituted of two different regions (cf. snapshots in the Table of Contents graphic).

Obviously this microscopic analysis is based on an energetic interpretation of the phenomena but it is relevant as hydrogen bond at room temperature represents a few k_BT. As temperature is increased this picture will lead to a more classical mixing behavior. Below we consider how this peculiar structural organization has an impact on dynamical properties.

DYNAMICAL ASPECTS AND LINK WITH MACROSCOPIC BEHAVIOR

We will present in this section both relaxation dynamics results and macroscopic transport coefficients. The computed viscosity was obtained from Green−Kubo's relation[49] on the stress tensor:

$$\eta = \frac{V}{k_BT}\int_0^\infty \mathrm{d}t\langle\sigma_{xy}(t)\cdot\sigma_{xy}(0)\rangle$$

with η the shear viscosity, k_B the Boltzmann constant, T the temperature, and σ_{xy} the (x,y) component of the stress tensor. To reduce statistical uncertainties, we used a modified version of this expression that can be found in refs 25 and 50:

$$\eta = \frac{V}{10k_BT}\lim_{\tau\to\infty}\int_0^\tau \mathrm{d}t\langle\sigma(0)\cdot\sigma(t)\rangle$$

where σ is the traceless and symmetric pressure tensor **P**.

Self-diffusion constants for each species were calculated from Einstein's relationship:

$$D_i = \lim_{t\to\infty}\frac{\mathrm{msd}_i(t)}{6t}$$

with D_i the self-diffusion constant of species i, t the time, and $\mathrm{msd}_i(t)$ the mean square displacement of species i. The time necessary to compute the self-diffusion coefficient is adjusted and changed with molar fraction. For each system we check that the $\mathrm{msd}(t)/6t$ reaches a plateau value and compute the self-diffusion constant on, at least, 1 ns of the plateau and up to 5 ns when needed.

Dynamical Transient Behavior. We present in Figure 7 various values of the $\mathrm{msd}_i(t)$ over $6t$. We consider the behavior

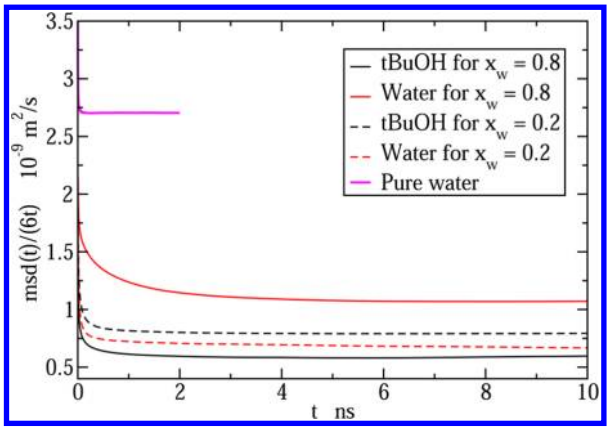

Figure 7. $\mathrm{msd}(t)/6t$ ratios for two water mole fractions: $x_w = 0.2$ and 0.8. Pure water is given as a reference.

of water and *tert*-butanol species in two different mixtures (x_w = 0.2 and 0.8). It is important to notice that a plateau is reached (corresponding to the Einstein diffusing regime) after only a few nanoseconds. The slowest relaxation is observed for water at $x_w = 0.8$. The behavior of pure water under the same conditions is shown for comparison: the plateau is reached after a few tenths of a nanosecond. To compute accurately the diffusion constants for finite size systems one should also compute viscosities and apply a hydrodynamic correction:[51]

$$D^\infty = D^L + \frac{k_BT\xi}{6\pi\eta L}$$

with D^∞ the diffusion coefficient for an infinite size system, D^L the diffusion coefficient calculated in a finite size system, η the viscosity (independent of the box size), L the box length, and ξ a hydrodynamic parameter depending only on box shape.

Here we encountered difficulties in computing the viscosities as the relaxation time scales of the structures in the fluid for high water proportions are very long (more than 30 ns) and thus stress tensor functions do not fully decorrelate at high water mole fractions. Therefore we cannot provide a reliable value of viscosity for all compositions from simulations. We present in the Supporting Information more details about the viscosities. Nevertheless, as we have quite large simulated boxes, we expect finite size effects to be rather small, and we present here diffusion constants without the hydrodynamic correction. These time scales represent the lifetimes of the structures discussed before in the paper. They might have been overestimated in the molecular dynamics simulations due to difficulties in describing transition states in the liquid.

dx.doi.org/10.1021/jp3124499 | J. Phys. Chem. B 2013, 117, 9718−9727

Dynamical Stationary Behavior. We present in Figure 8 the self-diffusion constants of the two species obtained from

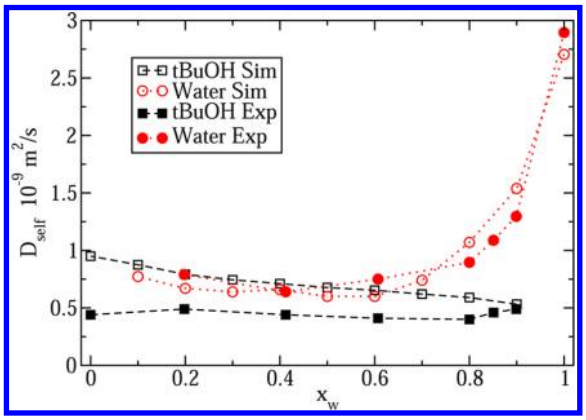

Figure 8. Evolution of the self-diffusion constants for the water and alcohol molecules as a function of water mole fraction.

both NMR experiments and equilibrium molecular dynamics. Agreement between the two sets of data is very good for water and qualitatively good for the alcohol. These results are also very close to those obtained by Price et al.[52] We note a very slow concentration dependence of the self-diffusion value of the alcohol, which can be related to two different effects: (a) The finite size effect: as the density is changing the box length changes so there is a small but existing effect on the diffusion constant. This effect is obviously very small as water self-diffusion coefficients are very well predicted. (b) A global density effect: molar volume of the mixture decreases in the system as the molar fraction of water increases so the fluid is more compact and, as expected, species will diffuse more slowly in a more compact system.

From these results on the self-diffusion coefficient of the alcohol we can conclude that the TraPPE-UA potential clearly overestimates this property. The evolution of water self-diffusion with composition can be interpreted in the light of the structural analysis done above. Let us consider water at infinite dilution in alcohol. Water molecules "adsorb" on alcohol hydrophilic sites and their dynamics is therefore strongly governed by alcohol molecule dynamics. Water molecule diffusion is notably restricted by the slower alcohol motion: the self-diffusion coefficient of water is much smaller than that of the pure water and is close to that of the alcohol. At large water concentration, both free and hydrogen bonded water molecules exist in the system and the water self-diffusion coefficient increases with increasing water contents. This dynamical crossover occurs at approximately $x_w = 2/3$, the molar fraction at which all association sites of the *tert*-butanol are occupied by water molecules and then form a "bulk"-like volume of water diffusing at the pure water dynamic.

The self-diffusion constant of water would then be equal to:

$$D_w^L = \psi_w^b D_{\text{bulk like}}^L + \tau \psi_w^a D_{HB}^L$$

with D_w^L the self-diffusion constant of water in a box of size L, $\psi_w^{a,b}$ respectively the absorbed-like and bulk-like water molecule fraction over all the water molecules in the system, D_{HB}^L the self-diffusion constant of water molecules H-bonded to the alcohol in a box of size L (slightly lower than the alcohol self-diffusion constant), $D_{\text{bulk like}}^L$ the self-diffusion constant of bulk-like water in a box of size L, and τ a scaling parameter close to 1, experimentally slightly higher than 1. This has been observed in other associated systems.[53−55]

Assuming again that the hydrodynamic correction is neglectable over the entire concentration we can write:

$$D_w = \psi_w^b D_{\text{bulk like}} + \tau \psi_w^a D_{HB}$$

To check this formula directly we can redraw the dependence of the self-diffusion coefficients in terms of the volume fraction instead of the mole fraction, as can be seen in Figure 9. We indeed note a linear behavior of the self-diffusion

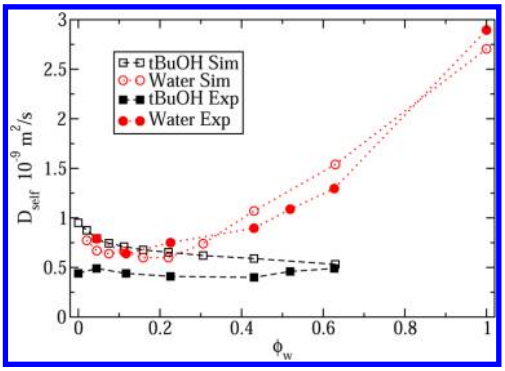

Figure 9. Self-diffusion constants of both water and alcohol molecules as a function of the water *volume* fraction.

constant of water in the "two phase" region. This is indirect evidence of our microscopic picture of mixing behavior in this associated fluid.

CONCLUSIONS

This work presents a general way to study miscibility phenomena in associated mixtures in which hydrogen bonds will strongly affect local structure. We performed long molecular dynamics simulations and neutron and X-ray experiments. This work was applied to a system documented in the literature: the water and *tert*-butanol mixture. Three different levels of results were obtained. First of all at a molecular level, hydrogen bonding is a driving force for clustering in the fluid. Small clusters of 4 molecules appear in the pure alcohol. The effect of adding water is to increase the size of the clusters (water molecules add to them) and also to widen distribution. Therefore we can understand both the shift of the "prepeak" at low q and the evolution of its width. At some point all the water molecules form a gigantic cluster: this is the percolation limit.

Then from these molecular structures the impact on mesoscopic phenomena is described: when adding water molecules to the pure alcohol, these water molecules will first of all hydrogen bond on the sites of the alcohol until all the sites are occupied and then they form an almost pure water phase in the system. We therefore identified mesoscopic nanophase separation at some water mole fraction. The limit of miscibility (or the microscopic limit of miscibility here) is observed at $x_w \approx 2/3$ above which the system forms large areas of almost pure water and alcohol. Nevertheless, the system is macroscopically miscible. A small change in the alcohol, or in the potentials used as reported by Gupta et al.,[44] could lead to macroscopic phase separation. All our observations imply that the various phenomena detailed in the literature (see for instance refs 44 and 56) at very high or very low water mole

dx.doi.org/10.1021/jp3124499 | J. Phys. Chem. B 2013, 117, 9718−9727

fractions are, in fact, consequences of the miscibility problem studied here.

Finally we showed how structural heterogeneities impact macroscopic behaviors on self-diffusion constants. The analysis consisting of dividing the water molecules into two different types allows us to predict the evolution of self-diffusion constants (for the water it presents a minimum value!).

Some important issues are still under consideration:

(a) From a dynamical point of view: the various relaxation times identified on the stress tensor (more than 30 ns) or the mean square displacement relaxation over time (around 10 ns) are unexpected in the mixture given the values for the two pure species.

(b) The structural properties: the topology of the clusters is not clear. The effect of the connectivity of the alcohol will dramatically affect the shape of the clusters (rings of limited connectivity possibilities or longer linear chains). Furthermore, the effect of the water on the structure has to be considered specifically.

(c) Many of the results are consequences of hydrogen bonding in the fluid. The effect of increasing temperature could also give a clue to the strength of hydrogen bonding between two different species (for instance: is there a temperature above which the self-diffusion constants present an "alkane"-like mixture behavior).

■ ASSOCIATED CONTENT

Supporting Information

Computed excess properties, some radial distribution functions, complementary simulated neutron and X-ray structure factors, neutron and X-ray experimental absolute intensities, experimental viscosities at various temperatures, sensitivity analysis of the clusters distribution computation, and some typical snapshots of different systems at low water content. This material is available free of charge via the Internet at http://pubs.acs.org.

■ AUTHOR INFORMATION

Corresponding Author

*E-mail: pierre-arnaud.artola@u-psud.fr (P.A.A.); christiane.alba-simionesco@cea.fr (C.A.-S.); and bernard.rousseau@u-psud.fr (B.R.).

Notes

The authors declare no competing financial interest.

■ ACKNOWLEDGMENTS

We would like to express our great appreciation to Jean-Marie Teuler for his upmost and valuable work on optimizing and parallelizing our molecular dynamics code. We would also like to thank Florence Porcher for her help with the experiments. This work was granted access to the HPC resources of IDRIS under the allocation 2012-2012096891 made by GENCI ("Grand Equipement National de Calcul Intensif"). We would like to thank Tom Fennell from the "Institut Laüe-Langevin" for his help. We thank the ANR (Agence Nationale de la Recherche) "blanc" for funding this project (StruDynaL, ANR-AA-PPPP-000). We would like to express our gratitude to all the undergratuated students that worked on this topic: Kevin Verstraete, Laétitia Pinaud, Nicolas Charrière, Grégoire Sergeant-Perthuis, Brice Maville, and Chloé Guilbaud.

■ REFERENCES

(1) Bakker, H. J. *Nature* **2012**, *491*, 533−535.
(2) Spector, M. S.; Selinger, J. V.; Schnur, J. M. *J. Am. Chem. Soc.* **1997**, *119*, 8533−8539.
(3) Koga, Y.; Nishikawa, K.; Westh, P. *J. Phys. Chem. A* **2004**, *108*, 3873−3877.
(4) Kiselev, M.; Ivlev, D. *J. Mol. Liq.* **2004**, *110*, 193−199.
(5) Lee, M. E.; Van der Vegt, N. F. A. *J. Chem. Theory Comput.* **2007**, *3*, 194−200.
(6) Wakisaka, A.; Ohki, T. *Faraday Discuss.* **2005**, *129*, 231−245.
(7) Guo, J. H.; Luo, Y.; Augustsson, A.; Kashtanov, S.; Rubensson, J. E.; Shuh, D. K.; Agren, H.; Nordgren, J. *Phys. Rev. Lett.* **2003**, *91*, 157401.
(8) Bowron, D. T.; Finney, J. L. *J. Phys. Chem. B* **2007**, *111*, 9838−9852.
(9) Cinelli, S.; Onori, G.; Santucci, A. *J. Phys. Chem. B* **1997**, *101*, 8029−8034.
(10) Dixit, S.; Crain, J.; Poon, W. C. K.; Finney, J. L.; Soper, A. K. *Nature* **2002**, *416*, 829−832.
(11) Houriez, C.; Masella, M.; Ferre, N. *J. Chem. Phys.* **2010**, *133*, 124508.
(12) Warshel, A. *Annu. Rev. Biophys. Biomol. Struct.* **2003**, *32*, 425−443.
(13) Kirkwood, J. G.; Boggs, E. M. *J. Chem. Phys.* **1942**, *10*, 394−402.
(14) Nieto-Draghi, C.; Avalos, J. B.; Rousseau, B. *J. Chem. Phys.* **2003**, *118*, 7954−7964.
(15) Ferrari, E. S.; Burton, R. C.; Davey, R. J.; Gavezzotti, A. *J. Comput. Chem.* **2006**, *27*, 1211−1219.
(16) Amore, S.; Horbach, J.; Egry, I. *J. Chem. Phys.* **2011**, *134*, 044515.
(17) Misawa, M.; Inamura, Y.; Hosaka, D.; Yamamuro, O. *J. Chem. Phys.* **2006**, *125*, 074502.
(18) Bravo-Sanchez, M. G.; Iglesias-Silva, G. A.; Estrada-Baltazar, A.; Hall, K. R. *J. Chem. Eng. Data* **2010**, *55*, 2310−2315.
(19) Wensink, E. J. W.; Hoffmann, A. C.; van Maaren, P. J.; van der Spoel, D. *J. Chem. Phys.* **2003**, *119*, 7308−7317.
(20) Harris, K. R.; Woolf, L. A. *J. Chem. Eng. Data* **2009**, *54*, 581−588.
(21) Abascal, J. L. F.; Vega, C. *J. Chem. Phys.* **2005**, *123*, 234505.
(22) Chen, B.; Potoff, J. J.; Siepmann, J. I. *J. Phys. Chem. B* **2001**, *105*, 3093−3104.
(23) Maerzke, K. A.; Schultz, N. E.; Ross, R. B.; Siepmann, J. I. *J. Phys. Chem. B* **2009**, *113*, 6415−6425.
(24) Allen, M. P.; Tildesley, D. *Computer Simulation of Liquids*; Clarendon Press: Oxford, United Kingdom, 1987.
(25) Thi, V. N.; Houriez, C.; Rousseau, B. *Phys. Chem. Chem. Phys.* **2010**, *12*, 930−6.
(26) Stewart, J. R.; Deen, P. P.; Andersen, K. H.; Schober, H.; Barthélémy, J. F.; Hillier, J. M.; Murani, A. P.; Hayes, T.; Lindenau, B. *J. Appl. Crystallogr.* **2009**, *42*, 69−84.
(27) Senanayake, P. C.; Gee, N.; Freeman, G. R. *Can. J. Chem.* **1987**, *65*, 2441−2446.
(28) Jerschow, A.; Muller, N. *J. Magn. Reson., Ser. A* **1996**, *123*, 222−225.
(29) Jerschow, A.; Muller, N. *J. Magn. Reson.* **1997**, *125*, 372−375.
(30) Barnes, A. C.; Fisher, H. E.; Salmon, P. S. *J. Phys. IV* **2003**, *111*, 59−96.
(31) Morineau, D.; Alba-Simionesco, C. *J. Chem. Phys.* **1998**, *109*, 8494−8503.
(32) Nath, P. P.; Sarkar, S.; Krishna, P. S. R.; Joarder, R. N. *Appl. Phys. A: Mater. Sci. Process.* **2002**, *74*, S348−S351.
(33) Kasraian, K.; Deluca, P. P. *Pharm. Res.* **1995**, *12*, 484−490.
(34) Asenbaum, A.; Pruner, C.; Wilhelm, E.; Mijakovic, M.; Zoranic, L.; Sokolic, F.; Kezic, B.; Perera, A. *Vib. Spectrosc.* **2012**, *60*, 102−106.
(35) Kezic, B.; Perera, A. *J. Chem. Phys.* **2012**, *137*, 014501.
(36) Palombo, F.; Paolantoni, M.; Sassi, P.; Morresi, A.; Cataliotti, R. S. *J. Mol. Liq.* **2006**, *125*, 139−146.
(37) Sassi, P.; Palombo, F.; Cataliotti, R. S.; Paolantoni, M.; Morresi, A. *J. Phys. Chem. A* **2007**, *111*, 6020−6027.

(38) Bowron, D. T.; Moreno, S. D. *J. Chem. Phys.* **2002**, *117*, 3753−3762.
(39) Finney, J. L.; Bowron, D. T.; Daniel, R. M.; Timmins, P.; Roberts, M. A. *Biophys. Chem.* **2003**, *105*, 391−409.
(40) Bowron, D. T.; Moreno, S. D. *J. Phys. Chem. B* **2005**, *109*, 16210−16218.
(41) Kirkwood, J. G.; Lewinson, V. A.; Alder, B. J. *J. Chem. Phys.* **1952**, *20*, 929−938.
(42) Shulgin, I.; Ruckenstein, E. *J. Phys. Chem. B* **1999**, *103*, 872−877.
(43) Shulgin, I. L.; Ruckenstein, E. *J. Phys. Chem. B* **2006**, *110*, 12707−12713.
(44) Gupta, R.; Patey, G. N. *J. Chem. Phys.* **2012**, *137*, 034509.
(45) Zhong, Y.; Patel, S. *J. Phys. Chem. B* **2010**, *114*, 11076−11092.
(46) Hands, M. D.; Slipchenko, L. V. *J. Phys. Chem. B* **2012**, *116*, 2775−2786.
(47) Artola, P. A.; Rousseau, B.; Galliero, G. *J. Am. Chem. Soc.* **2008**, *130*, 10963−10969.
(48) Bowron, D. T.; Finney, J. L.; Soper, A. K. *Mol. Phys.* **1998**, *93*, 531−543.
(49) Kubo, R.; Toda, M.; Hashitsume, N., *Statistical Physics II*, 3rd ed.; Springer-Verlag: Berlin, Germany, 1995.
(50) Daivis, P. J.; Evans, D. J. *J. Chem. Phys.* **1994**, *100*, 541−547.
(51) Yeh, I. C.; Hummer, G. *J. Phys. Chem. B* **2004**, *108*, 15873−15879.
(52) Price, W. S.; Ide, H.; Arata, Y. *J. Phys. Chem. A* **2003**, *107*, 4784−4789.
(53) Bedrov, D.; Borodin, O.; Smith, G. D. *J. Phys. Chem. B* **1998**, *102*, 9565.
(54) Borodin, O.; Bedrov, D.; Smith, G. D. *J. Phys. Chem. B* **2002**, *106*, 5194.
(55) Zhang, C.; Yang, X. *Fluid Phase Equilib.* **2005**, *231*, 1.
(56) Gazi, H. A. R.; Biswas, R. *J. Phys. Chem. A* **2011**, *115*, 2447−2455.